Journal of Materials Chemistry A

A Multi-Functional Interface Derived from Thiol-Modified Mesoporous Carbon in Lithium-Sulfur Batteries

Journal:	*Journal of Materials Chemistry A*
Manuscript ID	TA-ART-03-2019-002743.R1
Article Type:	Paper
Date Submitted by the Author:	25-Apr-2019
Complete List of Authors:	Li, Yun; University of Washington, Materials Science and Engineering Murphy, Ian; University of Washington, Department of Chemistry Chen, Ying; Pacific Northwest National Laboratory, Environmental Molecular Sciences Laboratory Lin, Francis; University of Washington, Department of Chemistry Wang, Xiang; University of Pittsburgh, Department of Mechanical Engineering and Materials Science Wang, Shanyu; University of Washington, Materials Science and Engineering Hubble, Dion; University of Washington, Molecular Engineering & Sciences Institute Jang, Sei-Hum; University of Washington, Materials Science and Engineering Mueller, Karl; Pacific Northwestern National Laboratory, Environmental Molecular Sciences Laboratory Wang, Chongmin; Pacific Northwest National laboratory, Environmental Molecular Sciences Laboratory Jen, Alex; University of Washington, Materials Science and Engineering; University of Washington, Chemistry Yang, Jihui; University of Washington, Materials Science and Engineering

Journal of Materials Chemistry A

ARTICLE

A Multi-Functional Interface Derived from Thiol-Modified Mesoporous Carbon in Lithium-Sulfur Batteries†

Received 00th January 20xx,
Accepted 00th January 20xx

DOI: 10.1039/x0xx00000x

www.rsc.org/

Yun Li,[‡a] Ian A. Murphy,[‡b] Ying Chen,[c] Francis Lin,[b] Xiang Wang,[d] Shanyu Wang,[a] Dion Hubble,[e] Sei-Hum Jang,[b] Karl T. Muller,[c] Chongmin Wang,[c] Alex K-Y. Jen,*[a,b,f] and Jihui Yang*[a]

Lithium-sulfur (Li-S) batteries hold great promise as a next-generation energy-storage technology. Their practical application, however, is hindered by the rapid capacity fade associated with the dissolution of lithium polysulfides (LiPSs) into the organic electrolytes. In this work, we successfully impede these losses by anchoring thiol (-SH) functional groups to the nonpolar surface of a mesoporous carbon host. This new strategy increases the surface polarity of the conductive carbons and traps LiPSs inside the cathodes. By utilizing various spectroscopic methods, we investigate the mechanisms of LiPSs trapping, which originate from the electrostatic and covalent interactions of the thiol functional groups with Li^+ from the electrolytes and with S from the LiPS chains, respectively. Here, we for the first time identify the multiple interactions that are induced by a small molecular interface upon cycling and correlate them with the electrochemical behavior. The fundamental insight on the thiol functionality suggests a further rational design of multi-functional interfaces to achieve better Li-S performance.

Introduction

Energy storage devices with high energy density are of increasing importance due to the growing demand for smart grid energy storage systems and long-range electric vehicles.[1,2] Lithium-sulfur (Li-S) batteries have attracted broad interest due to their high theoretical specific capacity (1672 mAh g^{-1}, an order of magnitude greater than that of the current commercial $LiCoO_2$ cathode material), low environmental impact, and low cost.[3] However, the commercialization of Li-S batteries has been hindered by multiple failure mechanisms which result in rapid capacity fading upon extended cycling.[4] This capacity fade is mainly caused by the dissolution of soluble lithium polysulfides (LiPSs) redox intermediates generated during the complex multi-step charge/discharge reactions.[5,6] Approaches which aim simply to lower LiPS solubility would introduce new performance deficits such as reduced reaction kinetics and poor active material utilization.[7,8] So as not to sacrifice general performance for the sake of cyclability, the design of cathode host materials which can better retain solvated LiPSs has become an area of intense research.[9]

Initial work on LiPS-trapping was focused on designing nanostructured carbon materials such as mesoporous carbon particles, carbon nanotubes (CNTs), graphene/graphene oxide sheets, etc.[10–18] Carbon materials were preferentially investigated as a means to physically confine solvated LiPSs in the host matrix due to their high electrical conductivity, large specific surface area, and ability to modulate the pore volume available for sulfur infiltration. Although these materials greatly improve cell performance, it has been found that physical confinement alone is not sufficient to prevent large capacity losses, as LiPSs will still gradually diffuse out of the porous network due to the polarity difference between non-polar carbon and polar LiPSs.[19] The non-polar carbon also introduces a new challenge, namely a poor electrolyte wetting for the thick electrodes.[19,20] Thus, research efforts have trended towards implementing chemical functionality to further improve a host material's ability to trap LiPSs. Most approaches implement inherently polar materials such as heteroatom-doped carbon structures,[21,22] polymer coatings,[23,24] metal-organic frameworks,[25,26] metal-chalcogenide blends,[27,28] etc. Although these approaches have realized some success in improving cyclability, they often rely only on limited and single electrostatic interaction, suffer reduced electrical conductivity, or involve heavy/expensive nanostructures, which sacrifice the potential advantages of Li-S chemistry.[10,29,30]

With all the challenges in mind, a light-weight sulfur host material with a good electrical conductivity and improved wettability to the electrolytes, that not only confines LiPSs physically but also contains a very high accessible fraction of

[a] Department of Materials Science and Engineering, University of Washington, Seattle, WA, 98195, USA.
[b] Department of Chemistry, University of Washington, Seattle, WA 98195, USA.
[c] Environmental Molecular Sciences Laboratory (EMSL), Pacific Northwestern National Laboratory, Richland, WA 99354, USA.
[d] Department of Mechanical Engineering and Materials Science, University of Pittsburgh, Pittsburgh, PA, 15261, USA.
[e] Molecular Engineering & Science, University of Washington, Seattle, WA 98195, USA.
[f] Department of Chemistry, City University of Hong Kong, Kowloon, HK.
* Email: jihuiy@uw.edu, ajen@uw.edu
‡ Both authors contributed equally to this work.
† Electronic Supplementary Information (ESI) available: Schematic of *in-situ* functionalization of modifiers; N_2 isotherms, XPS, SEM-EDS, TEM & TGA analysis for carbon and carbon/S composite with/without modifiers; Electrochemical performance, SEM, CV, NMR, contact angle analysis, & EIS of MJ430-S and SH-MJ430 cathodes; SEM-EDS of cycled Li metal; Table of selected Li-S batteries in comparison to this work. See DOI: 10.1039/x0xx00000x

LiPS chemisorption sites, is well-suited to realize long-life and high-loading Li–S batteries. To achieve the goal, in this work, we suggest to chemically functionalize the nonpolar surface of nanostructured carbon materials with a thin layer of phenylthiol small molecules via a one-pot reaction where we *in-situ* generate aryl-diazonium salts.[31] This approach has many benefits including simplicity, scalability, tunability, and general applicability to any surface with the sp^2 hybridized carbon functionality. Here we selected commercially available mesoporous carbon materials as the platform to study the features of phenylthiol surface modification. Graphene materials and CNTs were not considered due to their complexity such as the random orientation and discrepant defects of graphene sheets and the tedious synthetic and harsh reaction conditions to modify CNTs. [32–38] These obstacles make it difficult to stabilize and control the functionality of graphene materials and introduce large amounts of structural damages in CNTs.[35]

In the past few years, hydroxyl and epoxide functional groups have been reported to possess a single chemical interaction (O-Li) with LiPSs.[39–41] In this work, we for the first time designed phenylthiol modifiers at the molecular level on the surface of the carbon matrix to facilitate multiple interactions with LiPSs. Due to the widely-studied interconversion between the thiol (S-H) and disulfide (S-S) bonding modes through intermediate thiolates ($-S^-$) and thiyl radicals ($-S\bullet$),[42–45] thiol groups are chosen to potentially allow for covalent tethering of LiPSs to the surface of mesoporous carbon hosts. Furthermore, the thiol modifier could enhance the electrolyte wettability of electrodes by creating a more polar electrode surface, inducing electrostatic interactions with the solvated Li^+ ions of dissolved LiPSs, as well as lithium bis(trifluoromethanesulfonyl)imide (LiTFSI) salt in the 1,3-dioxolane/1,2-dimethoxythane (DOL/DME) based electrolytes. This effect has important implications for high-sulfur-loading cathodes, which are required for commercially viable cells and is often overlooked when discussing cathode additives/strategies.[19,20] The thiol-functionalized carbon host has not been studied probably because thiol functionality was predominantly consumed as reactive groups to prepare crosslinked organosulfur polymers in Li-S batteries.[46–48] These sulfur-rich polymers as a new cathode are chemically distinct from the conventional melt-infiltrated carbon-sulfur composites used in this work. The vulcanized co-polymers usually suffer from inherently low conductivity and require larger amounts of inert conductive additives, in addition to the inert mass added by the organic structures themselves, which detracts from the overall energy density.

In Li-S batteries, it is quite challenging for most materials to identify the specific role of individual species in cell function owing to the complexity in characterizing amorphous structures and versatile ionic species.[49] In this work, we successfully utilize solid-state Nuclear magnetic resonance (NMR) spectroscopy, X-ray photoelectron spectroscopy (XPS), and electrochemical impedance spectroscopy (EIS) to monitor the molecular motion and surface interactions of the thiol groups with active materials inside cathodes upon cycling. We studied the effects of the functionality on the electrochemical-produced LiPSs from the cycled cells, different from theoretical calculations or alternative investigation of the functionality with pre-made LiPS solutions of defined compositions.[16,40] Moreover, we conduct a systematic study of the influence of multi-functional thiol surfaces on high-sulfur-loading (4 mg cm^{-2}) cathodes by controlling the concentration of thiol groups on the surface. Though ultimately successful in improving cyclability, our analysis reveals some inherent limitations of this particular surface modification strategy, including a slight increase in cell overpotential and kinetic limitation during discharge. We thus present future steps that might be taken to mitigate these challenges.

Experimental

Preparation of [SH]-Thiol MJ430 Carbon

As-received MJ430 (Porous Carbon CNovelTM; TOYO TANSO USA, INC.) was purified by acid wash with 2M HCl in ethanol. Purified carbon powders were mixed with 5,10,15, 20, and 50 mol% 4-aminophenylthiol (Sigma Aldrich) and sonicated in anhydrous tetrahydrofuran for 20 min. This mixture was then placed in an ice bath before adding a stoichiometric equivalent of isoamylnitrite (Sigma Aldrich) and double stoichiometric equivalent of HCl to initiate *in-situ* diazotization. Initiation of the reaction should produce N_2 gas, which bubbles out of the solution. Once the gas generation has ceased, reaction mixture was heated to 70 ◦C and stirred vigorously for 12 h. Reaction products were cleaned and filtered with subsequent washes of (2:1) ethanol:ammonium hydroxide, tetrahydrofuran, water, and finally acetone. Cleaned products were then vacuum dried under high-vacuum at 90 ◦C for 12 h.

Material Characterization

Thermogravimetric analysis (TGA) was measured under a nitrogen flow of 50 mL/min with a heating rate of 10 °C min^{-1} to 800 °C by using a Mettler Toledo TFA/DSC 3+. Surface area of the samples was determined from the isotherms collected with a QUANTACHROME NOVA 2200e gas sorption system by using the BET method. The BJH method was used for the porosity and pore size analyses. Surface chemical characteristics of the samples were examined using XPS. Pass energy for survey and detail spectra (to calculate composition) was 150 eV. Data point spacing was 1.0 eV/step for survey spectra, and 0.4 eV/step for detail spectra. Pass energy for high-resolution spectra was 50 eV, with a data point spacing of 0.065 eV. The physiochemical structures were examined using a Renishaw inVia Raman Microscope. Electrical conductivity was measured by the four-point method using a IV SourceMeter (2450, Keithley). The MJ430-S and SH-MJ430-S films were fabricated by slurry casting method on polyethylene naphthalate (PEN). Morphology and elemental distribution of the materials were characterized using SEM-EDS (Phillips XL-30 Sirion FE-SEM with EDAX EDS). Microstructures and compositions were analyzed by S/TEM (FEI Titan 80-300kV, USA). Further experimental details are shown in Supplemental Information (ESI†).

Preparation of MJ430-S and [SH]-MJ430-S Composites

To impregnate sulfur into MJ430 or [SH]-MJ430 carbon for preparing MJ430-S or [SH]-MJ430-S, a mixture of 100 mg carbon and 100 mg sulfur was heated at 155 °C for 24 h in a sealed vacuum tube.

Electrochemical Measurements

The MJ430-S or [SH]-MJ430-S composite was mixed with Carbon Nanotubes (CNTs, Sigma-Aldrich) and poly(vinylidene difluoride) (PVDF; MTI Cop.) as the binder in a weight ratio of 80:10:10, in N-methyl-2-pyrrolidone (NMP; Sigma-Aldrich) as a dispersant. The slurry was cast on an Al foil current collector and dried overnight at 60 °C under vacuum. A thick cathode with 4 mg S cm^{-2} loading was prepared similarly. The slurry was casted on a C-coated Al foil current collector (MTI Corp.). 2032 coin-type cells were assembled using lithium metal (250 μm thick, Alfa Aesar) as the anode, polypropylene (PP) Celgard2500 (Celgard, LLC Corp) as the separator, and 1 M LiTFSI (Sigma-Aldrich) and 1 wt% $LiNO_3$ (Alfa Aesar) in DOL/DME (Sigma-Aldrich, v/v =1:1) as the electrolyte for each cell. The electrochemical performances of the cells were evaluated at 30 °C in a voltage window of 1.9-2.8 V vs. Li^+/Li at various C-rates using a battery tester (BT-2043, Arbin).

Spectroscopic Characterizations

Electrochemical impedance spectroscopy (EIS) of Li-S cells at different discharge stages were examined using an AMETEK VersaSTAT4 Potentiostat/Galvanostat in the frequency range of 10^{-2}-10^6 Hz by applying a 5 mV ac oscillation. ^7Li, ^{19}F, and ^{13}C MAS NMR were performed on a Varian Inova spectrometer with a 600 MHz (14.1 T) magnet, using 1.6 mm rotors operating at a spinning speed of 36 kHz. For the preparation of the first set of samples, the concentrated Li_2S_8 in DME with MJ430/20% SH-MJ430 particles were packed into the NMR rotors. For the second series of samples, the cycled coin cells were disassembled at different voltage stages in a glovebox, and the composites were scratched off from the cathodes immediately and filled into the NMR router. All XPS spectra were taken on a Surface Science Instruments S-Probe photoelectron spectrometer. Cycled cathode samples were disassembled in an Ar atmosphere glovebox, transferred to instrument in sealed vials, then mounted in ambient conditions. Further experimental details are shown in Supplemental Information (ESI†).

Results & discussion

Introduction of SH-MJ430 Carbon

As a platform to investigate our multifunctional interface, a commercially available mesoporous carbon host referred to as MJ430 was utilized, with an average surface area of 689 $m^2 g^{-1}$. A schematic depiction of our approach to confine active materials in the MJ430 pores using a multifunctional thiol surface modifier (SH-MJ430) is shown in Fig. 1. In our proposed strategy, there are three unique interactions occurring at the cathode interface which contribute to an increase in cell performance. The first is an electrostatic "lithium bond" between solvated Li^+ in the LiTFSI electrolyte and lone pairs on the reduced phenylthiolate moiety ($-S^-$). The second is a similar lithium bond involving the solvated Li^+ tails of dissolved LiPS. Finally, the third interaction is described as covalent disulfide bonding that is formed between $-S^-$ (or phenylthiyl radicals $-S\bullet$) and LiPSs. Evidence supporting each of these proposed interactions are present in the following sections.

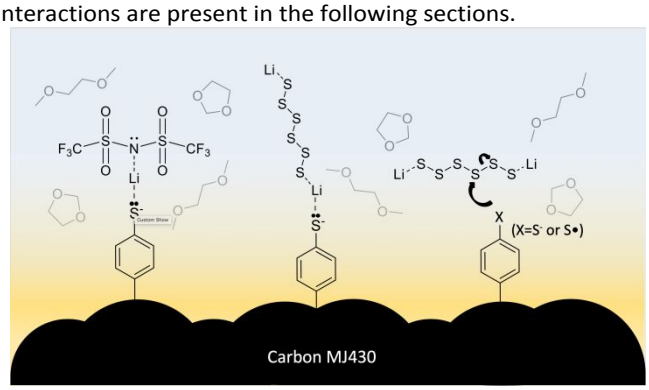

Fig. 1 Schematic depiction of the multiple interactions of thiol surface modifiers with solvated active materials. Proposed mechanisms include electrostatic interactions with Li^+ (left, middle), covalent disulfide bonding (right), and the subsequent attraction of solvent molecules to these aggregated charges.

Characterization of Functionalized SH-MJ430 Carbon

The functionalization of conductive carbon surfaces is made possible by a one-pot synthetic strategy that utilizes *in-situ* generated diazonium ions from common and inexpensive organic precursors.[31] We prepared a series of samples in which the concentration of surface modifiers was varied between 0 and 20 wt%. A mechanistic schematic of this reaction is shown in Fig. S1 (ESI†). We sought to confirm the functionalization by both physical and spectroscopic analyses, all of which are reported in Figs. 2 and 3. For these experiments, all "pristine" control samples were exposed to the same reaction conditions, barring the organic nitrite reagent which is necessary for diazotization. This was done to ensure the presence of functional groups was due to covalent anchoring to the surface, rather than physisorption or trapping of thiol precursors in the carbon pores. The addition of mass to carbon particles after a series of surface modification was tested by TGA (Fig. 2a). It was found that a maximum of ~ 20 wt% of mass could be added to pristine particles, as attempts to push reaction equilibrium even further towards functionalization (e.g. by adding 50 mol% diazonium precursors, instead of 20 mol%) yielded inconsequentially mass loss increase (Fig. S2 , ESI †). This finding may be attributed to a combination of precursor reactivity and the finite surface area readily available for attachment,[50] which would be optimized in the future such as by selecting other promising nanostructured carbons. Next, we confirmed that modifiers lined the pores of the host substrate through analysis of N_2 adsorption/desorption isotherms at 77K (Fig. S3, ESI †). From these N_2 isotherms with the Brunauer-Emmett-Teller (BET) and Barrett-Joyner-Halenda (BJH) analysis, an average surface area decreases from 689 to 310 $m^2 g^{-1}$ and a total pore volume (including all types of pores) decrease from 1.96 to 1.19 cc g^{-1} were observed after the maximum modification (Fig. 2b). The pore size distribution plots reveal a

gradual decrease in the primary mesopore size from 7.4 to 5.4 nm (Fig. S3f, ESI†). Moreover, the surface chemical composition of [SH]-MJ430 carbons was determined by XPS. The comparison of S_{2p} XPS spectra (Fig. 2c) clearly shows an increase in the S signal (observed at 164 eV) as the concentration of precursors is increased, which corresponds to the thiol species.[51] Fig. 2c is a detailed scan with a relatively low resolution (150 eV pass energy), which is meant to illustrate the intensity of the S signal. The high-resolution S_{2p} spectra (50 eV pass energy) are shown in Figs. S4c and S4e (ESI†). They suggest that only after exposure to the diazonium ions, a doublet peak centered at 164 eV can be observed, reflecting the anticipated spin-orbit splitting of aryl-thiol species after modification.[51] In Fig. S4a (ESI †), characteristic peaks of C and O atom clearly appear in both MJ430 and 20% SH-MJ430 spectra. Upon further analysis of high-resolution C_{1s} spectra (Figs. S4b and S4d, ESI†), the larger contribution of C-C signal in the 20% SH-MJ430 sample presumably results from the addition of C-C from the phenylthiol modifiers to MJ430. Finally, we tested for the degree of defects or disorders in the MJ430 mesoporous carbon before/after thiol modification by Raman spectrum shown in Fig. 2d. The intensity ratio of the D (~ 1357 cm^{-1}) and G (~ 1590 cm^{-1}) bands, I_D/I_G, slightly increases from 0.54 to 0.76 after the thiol modification, representing an increased defects/disorders of the mesoporous carbon and a decreased average size of the sp^2 conjugated domains in the carbon.[38,52] The relatively low increase in I_D/I_G value implies that our method results in limited damage to the conjugated structure of the pristine carbon matrix.[31,35] After thiol functionalization, the electrical conductivity of the cathode decreased slightly from 1.51 to 0.50 S cm^{-1}, but this value is still sufficiently high to make an electrochemically active electrode.[53]

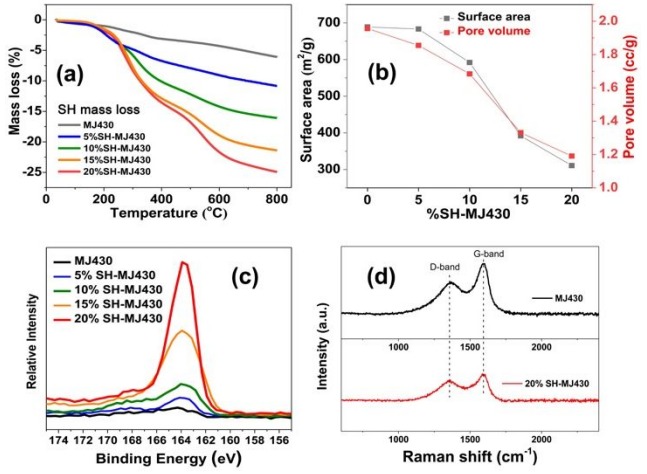

Fig. 2 Characterization of functionalized [SH]-MJ430 carbons ([SH] = 0, 5, 10, 15, 20 wt% SH), controlled via reaction conditions. (a) TGA analysis, (b) surface area and total pore volume attained from the N_2 isotherms analysis, and (c) XPS S_{2p} spectra of a series of [SH]-MJ430 carbons. (d) Raman spectra of MJ430 and 20% SH-MJ430 carbons.

Additional insight into how modification affects the physical nature of carbon particles was gained by imaging them using scanning electron microscopy (SEM) and scanning/transmission electron microscopy (S/TEM). No significant difference in carbon morphology was observed by SEM after modification, as is shown in Figs. 3a and 3d. TEM images show that the transparent mesopores in MJ430 (Figs. 3b, 3c, and S5a, ESI †) have turned into slightly turbid mesopores with thicker carbon walls after the thiol modification (Figs. 3e, 3f, and S5b, ESI†), revealing successful implementation of phenylthiol modifiers on the carbon surface. The average thickness of the carbon walls was obtained by examining eight different spots in TEM images (Figs. 3 and S5, ESI†). The value increases by about 1.4 nm after modification, from 1.82 nm to 3.22 nm, which agrees reasonably well with the reduced pore size presented in Fig. S3f (ESI†). The 1.4 nm increase of the carbon walls indicates a multi-layer structure of phenylthiol modifiers since the size of the mono-layer structure is estimated to be ~ 0.67 nm.[54] This multi-layer structure likely results from hyper-branching of diazonium intermediates during modification, a known process in this type of reaction.[55]

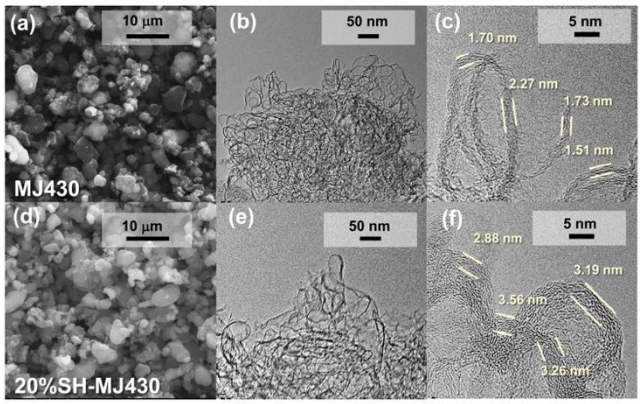

Fig. 3 SEM and TEM images of (a-c) MJ430 and (d-f) 20% SH-MJ430.

Electrochemical Performance of Li-S Batteries with SH-MJ430-S Cathodes

After characterization of the functionalized [SH]-MJ430 carbon, sulfur was infused into MJ430 and [SH]-MJ430 carbon to form MJ430-S and [SH]-MJ430-S composites. The exact weight content of sulfur in the composites was determined by TGA as shown in Fig. S6a (ESI†). The energy-dispersive spectra (EDS) confirm that the distinguishable S_8 particles (Fig. S7a, ESI †) would be encapsulated into the mesopores of 20% SH-MJ430 after being melted at 155 °C, showing uniform distribution of S in the 20% SH-MJ430-S (Fig. S7b, ESI†). It is consistent with the drastic decrease of the surface area and pore volume of the carbon matrix after sulfur infiltration, demonstrating good confinement of sulfur atoms inside carbon pores (Fig. S8, ESI†). The discharge/charge voltage profiles of MJ430-S and 20% SH-MJ430 cathodes at 0.05 C for the first 2 activation cycles and at 0.25 C for the following cycles (1C=1672 mA g^{-1}) are shown in Fig. 4a. Initially, a sulfur loading of ~ 1 mg cm^{-2} was utilized to compare with reported work on Li-S batteries, most of which use very thin (< 2 mg cm^{-2}) S electrodes.[10,27,46,47] The voltage profile features of the electrodes reflect those expected of a Li-S system, consisting of two discharge plateaus at 2.3 V and 2.1 V.[56] It is generally accepted that the upper plateau is related to a solid-liquid two phase conversion from elemental S_8 to long-

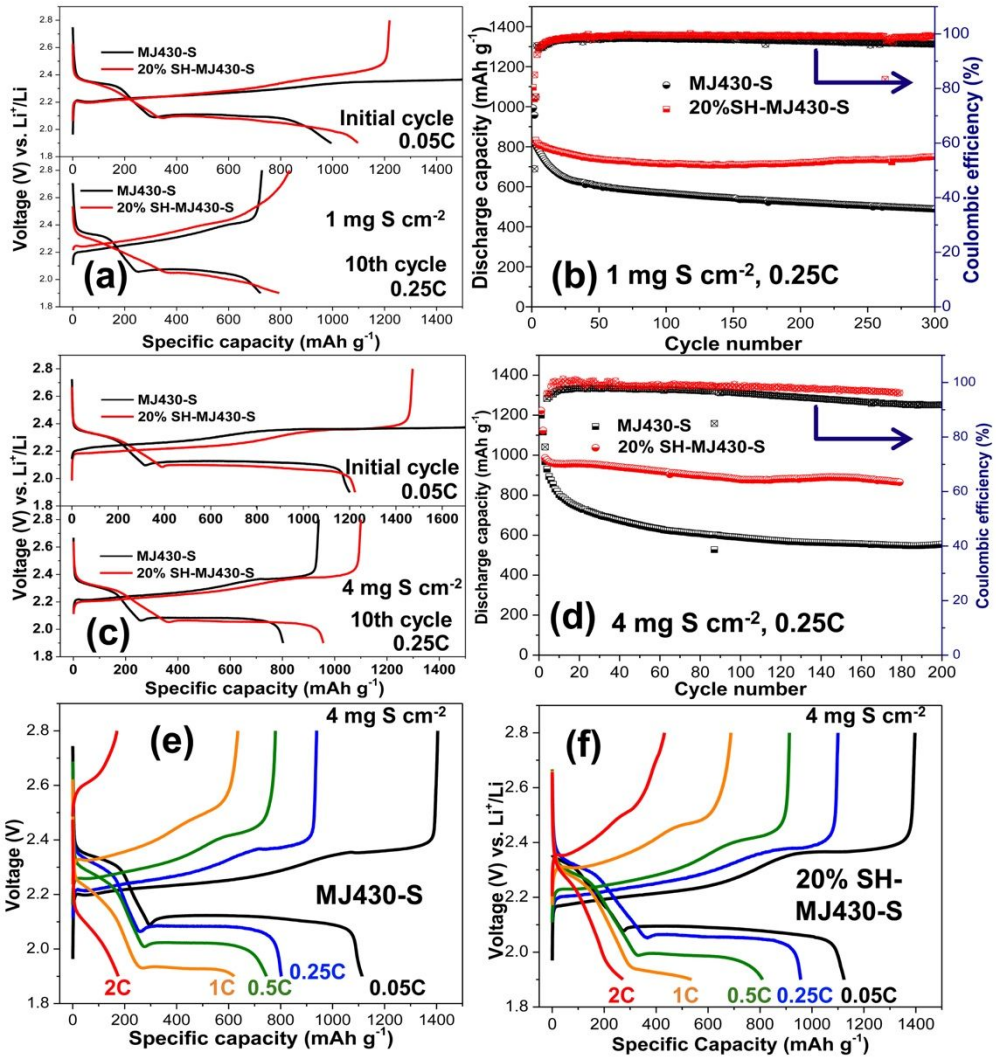

Fig. 4 (a) The discharge/charge voltage profiles of MJ430-S and 20% SH-MJ430-S electrodes based on a S loading of 1 mg cm^{-2} at the initial activation cycle (0.05 C) and the 10th cycle (0.25C) and (b) the corresponding cycling performance within the first 300 cycles. (c) The discharge/charge voltage profiles and (d) the corresponding cycling performance of MJ430-S and 20% SH-MJ430-S electrodes based on a S loading of 4 mg cm^{-2}. The discharge/charge voltage profiles of (e) MJ430-S and (f) 20% SH-MJ430-S electrodes at various rates.

chain $Li_2S_{(8,6)}$, while the lower is associated with a transition from liquid to solid-phase species as soluble chains are reduced to insoluble discharge products, $Li_2S_{(2,1)}$. In the initial charge process, the MJ430-S cathode shows an obvious overcharging behavior at 2.37 V, which is attributed to the occurrence of redox shuttling of dissolved LiPSs.[57,58] Briefly, the dissolved LiPSs escaping from the cathode, are continuously reduced at the anode and oxidized at the cathode, shuttling back and forth between each event. This behavior is inhibited in the 20% SH-MJ430-S cathode indicating an efficient protection of LiPS diffusion from the cathode to the Li anode, due to the interactions of the SH modifiers with LiPSs. Fig. 4b compares the corresponding long-term cycling performance of MJ430-S and 20% SH-MJ430-S cathodes. As expected, the modified cathode displays an obvious improvement in capacity retention. The capacity of the unmodified MJ430-S decreased from 812 to 486 mAh g^{-1} at 0.25 C (a capacity retention of 60%) after 300 cycles. Over the same number of cycles, the 20% SH-MJ430-S cathode shows a capacity retention of 89%, with the discharge capacity dropping from 838 to 745 mAh g^{-1}.

The enhanced capability of LiPS trapping in the 20% SH-MJ430-S cathode (1 mg S cm^{-2}) due to our modified surface allows us to address critical concerns in developing high-S-loaded Li-S cells, providing an effective means to increase areal capacity of the resultant batteries. The thiol modifier could also enhance the electrolyte wettability of electrodes by creating a more polar electrode surface, which is equally beneficial for the high-sulfur-loading cathodes. The electrochemical performance of MJ430-S and 20% SH-MJ430-S cathodes with a high sulfur loading of 4 mg cm^{-2} is evaluated in Figs. 4c and 4d. In Fig. 4c, the thick MJ430-S and 20% SH-MJ430-S cathodes deliver higher discharge capacities than the thin electrodes in Fig. 4a, due to the improved electrical conductivity of C-coated Al foil current collectors used in our high loading cells. More interestingly, the decreased coulombic efficiency of MJ430-S and 20% SH-MJ430-S cathodes (Fig. 4d) suggests a severe dissolution of LiPSs in the thick cathodes. After 180 cycles, the MJ430-S cells show a poor

cycling retention of 56% at 0.25C (556 mAh g^{-1}, Fig. 4d), whereas the capacity retention in the 20% SH-MJ430-S cells remains at 87% (865 mAh g^{-1}, Fig. 4d). We attribute the enhanced capacity retention of 20% SH-MJ430-S cells to the improved wettability and the restriction of LiPS dissolution in the modified cathode.

The rate capability of MJ430-S and 20% SH-MJ430-S cells is exhibited in Figs. 4e and 4f. After the activation cycles, the discharge capacities of 20% SH-MJ430-S at 0.05, 0.25, 0.5, 1, and 2C are 1121, 956, 811, 537, and 270 mAh g^{-1}, respectively. Upon close examination of the discharge curves of MJ430-S and 20% SH-MJ430-S cells, we can find an increased polarization in 20% SH-MJ430-S compared to MJ430-S especially for the second discharge plateau. This difference of the second discharge plateau is consistent with the distinction in the cyclic voltammogram of MJ430-S and 20% SH-MJ430-S cells (Fig. S9, ESI†). After modification, a distinction is recognized that the second reduction peak (~ 2.05 V for the MJ430-S) becomes broad and is shifted to ~ 2.02 V, which indicates that the thiol interface plays a significant role on the reduction of soluble LiPSs. The mechanism by which LiPSs dissolve and disproportionate will be further explored in following sections. Furthermore, to investigate the relationship between the thiol modifiers and the resultant electrochemical overpotentials, the electrochemical performance of [SH]-MJ430-S cathodes ([SH]= 0, 5, 10, 15, 20 wt% SH) is investigated in Figs. S6b and S6c (ESI †). A gradual reduction in overpotential was observed as the concentration of SH modifier decreases (Fig. S6b, ESI†), whereas 20wt% SH-MJ430-S still displays the highest discharge capacity after long-term cycling (Fig. S6c, ESI †). Moreover, the SEM images of cycled 20% SH-MJ430-S cathodes (Fig S10, ESI†) show less pulverization of carbon particles upon repeated cycling, suggesting that the amorphous surface film produced by our modifiers can also enhance the long-term mechanical integrity of the electrode.

The thick cells were discharged at a relatively low rate (0.25 C) to prevent the problems of Li anode during cycling, including dendrite formation, pulverization, and solid electrolyte interphase buildup.[19] The SEM images of the Li metal surface before and after long-term cycling are shown in Fig. S11 (ESI†). In comparison to the rough surface with thick passive interphase in the MJ430-S cell (Fig. S11b, ESI†), the cell with 20% SH-MJ430-S cathode showed a smoother surface of Li metal (Fig. S11c, ESI†), although it was still covered by some particles, the so-called lithium dendrites.[59] The severe passive interphase in the MJ430-S cell is probably formed by the reaction of dissolved LiPSs with the Li and electrolytes. Future work associated with the anode will be pursued to achieve high discharge/charge current densities.[60–62]

The electrochemical performance of 20% SH-MJ430-S with a high sulfur loading resembles those of the state-of-the-art Li-S battery systems, as list in Table S1 (ESI†). In the future, we will explore the surface modification of other highly sp^2-hybridized carbons (e.g. CNTs) to provide an interconnected conductive scaffold, reduce polarization, and achieve higher energy densities in particular for the long-term cycle performance of Li-S batteries. In this work, however, considering the complexity of surface modification of CNTs and graphene as mentioned in the introduction, we adopt the mesoporous carbon matrix as the platform to isolate the additional effects of CNTs and graphene on the SH-modified cells, even though the mesoporous carbon matrix would compromise the overall cycling performance of Li-S batteries.

Spectroscopic Analysis of Interactions between Solvated Active Materials and Electrode Surfaces

NMR As discussed above, the improved capacity retention of MJ430-S cathodes with thiol modifiers is presumed to strongly correspond to the multifunctional interactions on the thiol surface, especially during the second discharge stage. To verify our postulated electrostatic interactions of the thiol groups with active materials, solid-state magic angle spinning (MAS) NMR was performed on various samples to reveal the changes in the atomic environments. Here ^{7}Li, ^{13}C, and ^{19}F NMR were collected on two sets of samples to probe the various possible interactions. In the first set, the ^{7}Li spectra shows the interactions of MJ430/20% SH-MJ430 carbon with a concentrated Li_2S_8 solution in DME. In Fig. 5a, the spectra of both samples can be fit using two Lorentzian peaks. Here we assign the upfield resonance at -1 ppm to long chain Li_2S_n (n = 6, 8), and the downfield resonance at around 0 ppm to its short chain byproducts Li_2S_n (n = 2, 4) of the dynamic equilibrium in LiPS solutions.[63] It has been both theoretically and experimentally documented that Li^+ coordinated by the Lewis-basic donors results in a downfield shift of around 0.5 ppm,[64] so this shift (from MJ430 to 20% SH-MJ430) was attributed to be the formation of electrostatic Li bonds between the terminal Li in LiPSs and the filled p-orbitals of S from the thiol surface. This result suggests that our surface modifiers can interact with LiPSs in organic solvents even without applying an external bias to electrochemically drive disulfide bonding.

To further understand the effect of a thiol surface on battery performance, our second set of samples are cathode materials from cycled cells discharged to different voltages (1.9 V and 2.1 V). All the samples are acquired without them being washed to capture both soluble and insoluble species. Fig. 5b shows ^{7}Li MAS NMR spectra after normalizing to the weight of active materials packed in rotors. While the resonances at 2.5 ppm and 1.2 ppm are attributed to solid Li_2S and solid Li_2S_n, respectively,[65] the relatively broad peak at -1 ppm includes the signals from solution Li_2S_n and LiTFSI that is confined on the carbon surface or inside the nanoscale pores.[7] ^{19}F signal at around -80 ppm and 13C signal at -121 ppm in Fig. S12 (ESI†) both confirm the presence of confined LiTFSI solution. The relatively sharp ^{7}Li signal at around -1 ppm (Fig. 5b) shown only in 20% SH-MJ430-S suggests the existence of mobile Li^+ species surrounded by solvent molecules in the modified cathodes. As a result, the existence of mobile Li^+ species implies that the surface modification improves integration of electrolyte into the cathode matrix, probably due to the dipole-dipole interaction of thiol groups with solvated Li^+ and with polar molecules or moieties from the electrolyte. The improved wettability was further confirmed by the contact angle analysis in Fig. S13 (ESI†), which suggests stronger adhesion between the electrolyte and the 20% SH-MJ430-S than that at the

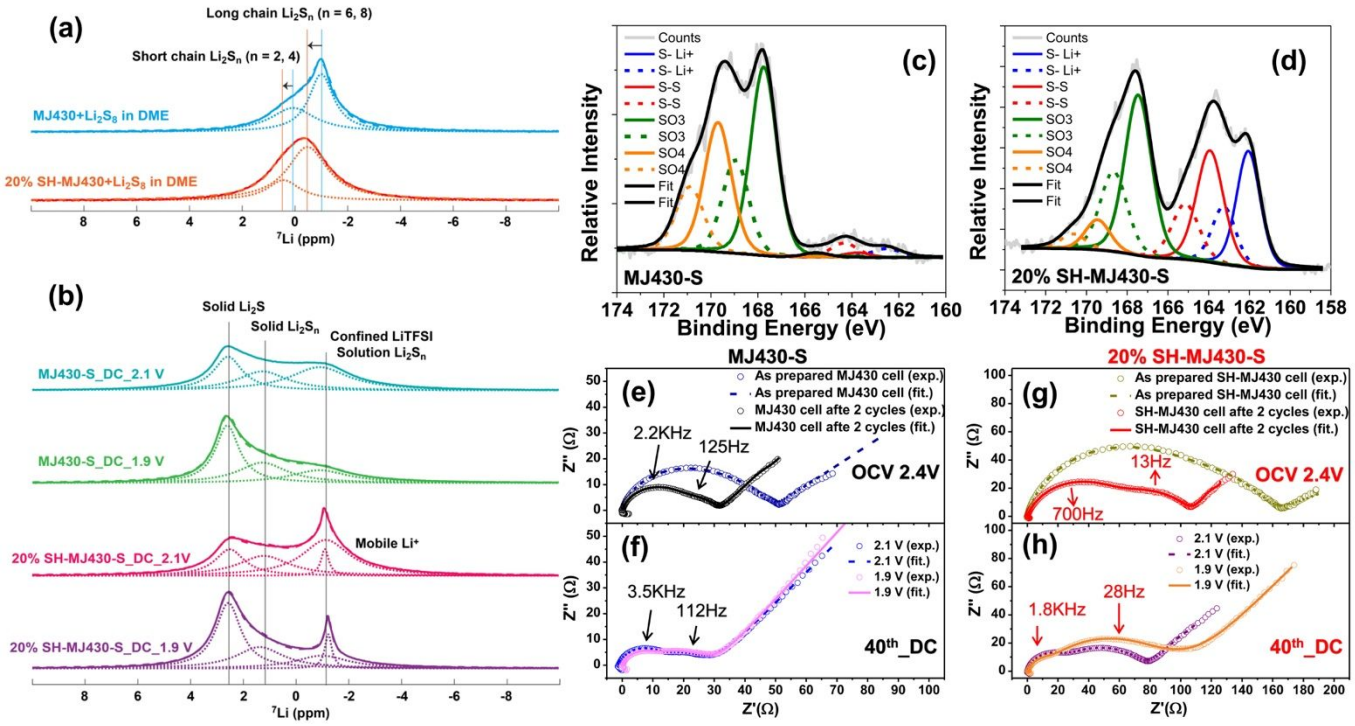

Fig. 5 (a) ^{7}Li MAS NMR spectra of Li_2S_8 solution interacting with the MJ430 and 20% SH-MJ430. (b) ^{7}Li MAS NMR spectra of cathode materials with the MJ430-S and 20% SH-MJ430-S from Li-S cells that are discharged to different voltages, with experimental data in solid lines, deconvolution peaks in dot lines, and the sum of deconvolution peaks in dash lines. High resolution S_{2p} XPS spectra of (c) MJ430-S and (d) 20% SH-MJ430-S cathodes, obtained from Li-S cells discharged to 1.9 V after 100 cycles. EIS analysis of (e-f) MJ430-S and (g-h) 20% SH-MJ430-S cells at different stages of discharge within 40 cycles.

electrolyte and the MJ430-S interface. This effect could lead to improved utilization of active materials during cycling, since better access to the electrolyte within pores would aid in solvation and confinement of solvated LiPSs. It is consistent with the integration area of each deconvolution peak in Fig. 5b (Table S2, ESI †), which shows that the amount of LiPSs and LiTFSI increases by 50% in the modified electrode when discharged to 2.1 V and these LiPSs are further reduced to solid Li_2S at 1.9 V increasing the accumulation of Li_2S. The downfield chemical shift at -1 ppm in the powder materials (Fig. 5a) is not observed in the cycled cells (Fig. 5b), perhaps due to the fact that Li^+ is in great excess to the SH-thiol modifiers in the cycled cells (~ 1 Li^+ to 0.1 SH). Therefore, the electrostatic Li bond does not contribute as significantly as in the powder materials where Li^+ is comparable to the SH-thiol modifiers (~ 1 Li^+ to 1.6 SH)

XPS With strong evidence to support the reaction mechanisms through changes in Li^+ environment, we utilized XPS to spectroscopically identify changes of sulfur speciation in cycled cathodes. Although S_{2p} high-resolution analysis can determine the difference between S-S bonds (S^0; 164eV) and S^-Li^+ bonds (S^{-1}; 161eV),[66–68] it cannot distinguish between physiosorbed and chemically anchored S species. Thus, to minimize convolution from non-surface bound sulfur species, cycled cathodes were thoroughly washed with DOL/DME to remove any soluble sulfur species, which presumably includes all polysulfides not bound to the surface. The comparative photoelectron spectra of modified and pristine cathodes are shown in Figs. 5c and 5d. The successful removal of non-surface-bound sulfur species was confirmed by the unmodified cathode spectrum, Fig. 5c. Only very minor photoelectron signals at 161 or 164 eV, which correspond to the tail and core sulfur species of LiPS, respectively, are detectable, indicating that virtually all free LiPSs has been removed. This is in contrast with the spectra in Fig. 5d, which shows a large signal for both states of sulfur, suggesting that despite thorough washing, LiPS chains remain tethered to the electrode surface with the thiol modifiers via covalent disulfide bonds. During repeated discharge/charge processes, the thiol modifiers are primarily regarded as thiolates ($-S^-$) and thiyl radicals ($-S\bullet$) in the electrochemical system.[44] The oxidized species in both XPS samples are of indefinite origin; however, we note that a sulfite (SO^{3-}) signal at 167 eV is detectable even in as-received carbon samples, potentially indicating its origin as a byproduct of manufacturing, rather than cell-related processes.

EIS In our cells, we observe an additional rate-dependent overpotential in modified cathodes (Fig. 4), which is indicative of a kinetic-limiting chemical reaction occurring as a result of thiol modification. To further discern this influence, EIS was performed on the cells with/without SH modifiers at different stages of discharge within 40 cycles. The Nyquist plots are shown in Fig. 5e-h and Fig. S14a-f (ESI †). In order to obtain mechanistic insights from these plots, we fitted the impedance data using an electric equivalent circuit (EEC, Fig. S14g, ESI†) and the element values derived from the EEC fit are summarized in Figs. S14g and S14h.

By comparing the plots of as prepared cells held at the open circuit (Figs. 5e and 5g), we observed that the high-frequency interphase resistance (R_i) of 20% SH-MJ430-S cathode ($R_{i,fresh,SH}$

=104.5 Ω) is three-fold higher than that of the cells with MJ430-S cathodes ($R_{i,fresh}$ =31.8 Ω). The large increase in $R_{i,fresh}$ after the modification is primarily ascribed to the reduced lithium diffusion in the thicker surface film produced by the modification. After two formation cycles, R_i of both MJ430-S and 20% SH-MJ430-S cells dramatically decrease, likely attributable to the redistribution of sulfur species on the surface of the carbon host, allowing for better interface contacts. In contrast, the mid-frequency charge transfer resistance (R_{ct}) of 20% SH-MJ430-S cathode quickly increases ($R_{ct,fresh,SH}$ =17.7 Ω vs. $R_{ct,2nd,SH}$ = 49.4 Ω) and continues growing to 70-80 Ω in the following cycles (Fig. 5h and Fig. S14d-f, ESI†), while R_{ct} of the cell with MJ430-S cathode remains constant (~ 15 Ω) upon cycling. The growth of $R_{ct,SH}$ is likely related to the kinetically limiting formation of covalent disulfide bonds with thiol modifiers. Additionally, we notice a ~ 10 Ω increase in $R_{ct,SH}$ when the 20% SH-MJ430-S cell is discharged from 2.1 to 1.9 V (Fig. 5h). We hypothesized that the increased resistance at lower potentials may be caused in part by an increasing activation barrier for further reduction of polysulfide chains tethered to the surface. Therefore, we suggest that the kinetic limitation after the modification is partially due to the need to drive additional surface reactions (formation of disulfide bonding), and partially due to a thickening of the dynamic semi-solid layer of active material within cathode pores (a result of more, and stronger, interaction modes with LiPSs), which hinders Li^+ diffusion within the carbon matrix.

Conclusions

In summary, the utility of a thiol-based, multifunctional, redox-active interface has been demonstrated for LiPS-trapping and improving electrolyte wetting in the C/S composite electrodes for Li-S batteries. This was achieved through a highly flexible synthetic method which grafts organic molecules onto the surface of conductive carbon host materials, allowing for variability in both desired functionality and degree of functionalization. In this study, we showed that thiol surfaces could interact with solvated active materials in multiple ways, including covalent interactions and electrostatic lithium bonding. Additionally, the polar, nucleophilic surface introduced by the thiol modifiers allowed for better wetting of the electrode surface by the electrolytes due to the dipole-dipole interaction of the thiol groups with Li^+ from the electrolyte. This improved wettability allows for better sulfur utilization in high loading (4 mg cm^{-2}) cells while maintaining the tethering of solvated LiPSs to the cathode surface. The realization of multiple performance enhancements from a single functional group suggests the possibility of further rational molecular design of cathode systems based on small molecule interfaces. In the future, we will plan to explore the potential of altering the molecular structure of modifiers and investigate other carbon matrices. For example, a dithiol molecular functionalization could be considered to improve the reaction kinetics, as several dithiols have been reported to catalyze the reduction of polysulfides in chemical or biochemical systems.[36,45]

Conflicts of interest

There are no conflicts to declare.

Acknowledgements

This work is based upon work supported by the Department of Energy, Office of Energy Efficiency and Renewable Energy (EERE), under Award Number DE-EE0007791. NMR and TEM measurements are supported by the Environmental Molecular Sciences Laboratory (EMSL), a national scientific user facility sponsored by the U.S. Department of Energy's Office of Biological and Environmental Research and located at Pacific Northwest National Laboratory (PNNL). Part of this work was conducted at the Washington Clean Energy Testbeds, a facility operated by the University of Washington Clean Energy Institute. It was also conducted at the Molecular Analysis Facility, a National Nanotechnology Coordinated Infrastructure site at the University of Washington which is supported in part by the National Science Foundation (grant ECC-1542101), the University of Washington, the Molecular Engineering & Sciences Institute, the Clean Energy Institute, and the National Institutes of Health. A special thanks to Dr. Gerry Hammer for aiding in the collection and interpretation of XPS spectra.

Author Contributions

Y.L., I.M., D.H., A.J., and J.Y. proposed the research. Y.L., I.M., S.J., and J.Y. designed the experiments. F.L. and I.M. performed the carbon modification. I.M. analyzed the XPS measurements. Y.L. performed the material characterizations (except XPS), the electrochemical measurements, and EIS tests. X.W. and C.W. conducted the S/TEM measurement. S.W. and Y.L. conducted SEM characterization. Y.C. and K.M. conducted the NMR measurement. Y.L., I.M., A.J., and J.Y. co-wrote the paper. All authors discussed the results and commented on the manuscript.

Notes and references

1 B. Dunn, H. Kamath and J.-M. M. Tarascon, *Science* , 2011, **334**, 928–935.

2 D. Howell, *Meeting Abstracts, The Electro. Soc.,* 2016, No. 1, pp. 2-2.

3 J. B. Goodenough and K. S. Park, *J. Am. Chem. Soc.*, 2013, 135, 1167–1176.

4 M. Hagen, D. Hanselmann, K. Ahlbrecht, R. Maça, D. Gerber and J. Tübke, *Adv. Energy Mater.*, 2015, **5**, 1401986.

5 G. Li, S. Wang, Y. Zhang, M. Li, Z. Chen and J. Lu, *Adv. Mater.*, 2018, **1705590**, 1–19.

6 R. Xu, J. Lu and K. Amine, *Adv. Energy Mater.*, 2015, 5, 1500408.

7 J. Chen, K. S. Han, W. A. Henderson, K. C. Lau, M. Vijayakumar, T. Dzwiniel, H. Pan, L. A. Curtiss, J. Xiao, K. T. Mueller, Y. Shao and J. Liu, *Adv. Energy Mater.*, 2016, **6**, 1600160.

8 S. Zhang, A. Ikoma, Z. Li, K. Ueno, X. Ma, K. Dokko and M.

Watanabe, *ACS Appl. Mater. Interfaces*, 2016, **8**, 27803–27813.

9 A. Eftekhari and D.-W. Kim, *J. Mater. Chem. A*, 2017, **5(34)**, 17734-17776

10 Q. Pang, X. Liang, C. Y. Kwok and L. F. Nazar, *Nat. Energy*, 2016, 1, 16132.

11 X. Ji, K. T. Lee and L. F. Nazar, *Nat. Mater.*, 2009, **8**, 500–506.

12 Z. Li, H. Bin Wu and X. W. Lou, *Energy Environ. Sci.*, 2016, 9, 3061–3070.

13 S. Evers and L. F. Nazar, *Chem. Commun.*, 2012, **48**, 1233–1235.

14 T. Fujimori, A. Morelos-Gómez, Z. Zhu, H. Muramatsu, R. Futamura, K. Urita, M. Terrones, T. Hayashi, M. Endo, S. Young Hong, Y. Chul Choi, D. Tománek and K. Kaneko, *Nat. Commun.*, 2013, **4**, 2162.

15 Z. Yuan, H. J. Peng, J. Q. Huang, X. Y. Liu, D. W. Wang, X. B. Cheng and Q. Zhang, *Adv. Funct. Mater.*, 2014, **24**, 6105–6112.

16 F. Wang, X. Ding, R. Shi, M. Li, Y. Lei, Z. Lei, G. Jiang, F. Xu, H. Wang, L. Jia, R. Jiang, Z. Liu and J. Sun, *J. Mater. Chem. A*, , DOI:10.1039/C9TA00544G.

17 H. Li, Y. Tao, C. Zhang, D. Liu, J. Luo, W. Fan, Y. Xu, Y. Li, C. You, Z.-Z. Pan, M. Ye, Z. Chen, Z. Dong, D.-W. Wang, F. Kang, J. Lu and Q.-H. Yang, *Adv. Energy Mater.*, 2018, **8**, 1703438.

18 C. Hernández-Rentero, R. Córdoba, N. Moreno, A. Caballero, J. Morales, M. Olivares-Marín and V. Gómez-Serrano, *Nano Res.*, 2018, **11**, 89–100.

19 J. Lochala, D. Liu, B. Wu, C. Robinson and J. Xiao, *ACS Appl. Mater. Interfaces*, 2017, **9**, 24407–24421.

20 D. Lv, J. Zheng, Q. Li, X. Xie, S. Ferrara, Z. Nie, L. B. Mehdi, N. D. Browning, J. G. Zhang, G. L. Graff, J. Liu and J. Xiao, *Adv. Energy Mater.*, 2015, **5**, 1402290.

21 J. Zhang, Y. Shi, Y. Ding, L. Peng, W. Zhang and G. Yu, *Adv. Energy Mater.*, 2017, **7**, 1602876.

22 Z. Xiao, Z. Yang, L. Zhang, H. Pan and R. Wang, *ACS Nano*, 2017, **11**, 8488–8498.

23 W. Zhou, H. Chen, Y. Yu, D. Wang, Z. Cui, F. J. Disalvo and H. D. Abruña, *ACS Nano*, 2013, **7**, 8801–8808.

24 H. Chen, W. Dong, J. Ge, C. Wang, X. Wu, W. Lu and L. Chen, *Sci. Rep.*, 2013, **3**, 1910.

25 W. Xia, A. Mahmood, R. Zou and Q. Xu, *Energy Environ. Sci.*, 2015, **8**, 1837–1866.

26 J. Zhou, X. Yu, X. Fan, X. Wang, H. Li, Y. Zhang, W. Li, J. Zheng, B. Wang and X. Li, *J. Mater. Chem. A*, 2015, **3**, 8272–8275.

27 X. Liu, J.-Q. Huang, Q. Zhang and L. Mai, *Adv. Mater.*, 2017, **29**, 1601759.

28 F. Pei, L. Lin, A. Fu, S. Mo, D. Ou, X. Fang and N. Zheng, *Joule*, 2018, **2**, 323–336.

29 Z. W. Seh, Y. Sun, Q. Zhang and Y. Cui, *Chem. Soc. Rev.*, 2016, 45, 5605–5634.

30 Q. Pang, X. Liang, C. Y. Kwok and L. F. Nazar, *J. Electrochem. Soc.*, 2015, **162**, A2567–A2576.

31 J. H. Kim, T. Kim, Y. C. Jeong, K. Lee, K. T. Park, S. J. Yang and C. R. Park, *Adv. Energy Mater.*, 2015, **5**, 1500268.

32 M. K. Song, Y. Zhang and E. J. Cairns, *Nano Lett.*, 2013, **13**, 5891–5899.

33 Z. Sun, J. Zhang, L. Yin, G. Hu, R. Fang, H. M. Cheng and F. Li, *Nat. Commun.*, 2017, **8**, 14627.

34 M. Shaibani, A. Akbari, P. Sheath, C. D. Easton, P. C. Banerjee, K. Konstas, A. Fakhfouri, M. Barghamadi, M. M. Musameh, A. S. Best, T. Rüther, P. J. Mahon, M. R. Hill, A. F. Hollenkamp and M. Majumder, *ACS Nano*, 2016, **10**, 7768–7779.

35 J. Mao, Y. Wang, J. Zhu, J. Yu and Z. Hu, *Appl. Surf. Sci.*, 2018, **447**, 235–243.

36 W. Hua, Z. Yang, H. Nie, Z. Li, J. Yang, Z. Guo, C. Ruan, X. Chen and S. Huang, *ACS Nano*, 2017, **11**, 2209–2218.

37 R. Ponraj, A. G. Kannan, J. H. Ahn, J. H. Lee, J. Kang, B. Han and D. W. Kim, *ACS Appl. Mater. Interfaces*, 2017, **9**, 38445–38454.

38 L. Ma, H. L. Zhuang, S. Wei, K. E. Hendrickson, M. S. Kim, G. Cohn, R. G. Hennig and L. A. Archer, *ACS Nano*, 2016, **10**, 1050–1059.

39 G. Zhou, L.-C. Yin, D.-W. Wang, L. Li, S. Pei, I. R. Gentle, F. Li and H.-M. Cheng, *ACS Nano*, 2013, **7**, 5367–5375.

40 G. Zhou, E. Paek, G. S. Hwang and A. Manthiram, *Nat. Commun.*, 2015, **6**, 7760.

41 C. H. Chang and A. Manthiram, *ACS Energy Lett.*, 2018, **3**, 72–77.

42 M. Liu, S. J. Visco and L. C. De Jonghe, *J. Electrochem. Soc.*, 1989, **136**, 2570–2575.

43 A. Joseph and B. George, *Rubber Sci.*, 2016, **29(1)**, 62–100.

44 M. Borsari, M. Cannio and G. Gavioli, *Electroanalysis*, 2003, **15**, 1192–1197.

45 G. V. Lamoureux and G. M. Whitesides, *J. Org. Chem.*, 1993, **58**, 633–641.

46 N. Xu, T. Qian, X. Liu, J. Liu, Y. Chen and C. Yan, *Nano Lett.*, 2017, **17**, 538–543.

47 H. Kim, J. Lee, H. Ahn, O. Kim and M. J. Park, *Nat. Commun.*, 2015, **6**, 7278.

48 S. Choudhury, P. Srimuk, K. Raju, A. Tolosa, S. Fleischmann, M. Zeiger, K. I. Ozoemena, L. Borchardt and V. Presser, *Sustain. Energy Fuels*, 2018, **2**, 133–146.

49 A. Hoefling, D. T. Nguyen, P. Partovi-Azar, D. Sebastiani, P. Theato, S.-W. Song and Y. J. Lee, *Chem. Mater.*, 2018, 30, 2915-2923

50 M. Toupin and D. Bélanger, *Langmuir*, 2008, **24**, 1910–1917.

51 D. G. Castner, K. Hinds and D. W. Grainger, *Langmuir,* 2002, **12(21)**, 5083-5086

52 G. Li, J. Sun, W. Hou, S. Jiang, Y. Huang and J. Geng, *Nat. Commun.*, 2016, **7**, 10601.

53 S. J. Kwon, C. W. Kim, W. T. Jeong and K. S. Lee, *J. Power Sources*, 2004, **137**, 93–99.

54 I. G. Dance, K. J. Fisher and R. M. Herath Banda, *Inorg. Chem.*, 1991, vol. 30., 183-187

55 P. Viel, X. T. Le, V. Huc, J. Bar, A. Benedetto, A. Le Goff, A. Filoramo, D. Alamarguy, S. Noël, L. Baraton and S. Palacin, *J. Mater. Chem.*, 2008, **18**, 5913–5920.

56 A. Manthiram, Y. Fu, S.-H. Chung, C. Zu and Y.-S. Su, *Chem. Rev.*, 2014, **114**, 11751–11787.

57 J. W. Park, K. Yamauchi, E. Takashima, N. Tachikawa, K. Ueno, K. Dokko and M. Watanabe, *J. Phys. Chem. C*, 2013, **117**, 4431–4440.

58 Y. V. Mikhaylik and J. R. Akridge, *J. Electrochem. Soc.*, 2004, **151**, A1969.

59 S. H. Kim, J. S. Yeon, R. Kim, K. M. Choi and H. S. Park, *J. Mater. Chem. A*, 2018, **6**, 24971–24978.

60 X. Hu, X. Sun, S. J. Yoo, B. Evanko, F. Fan, S. Cai, C. Zheng, W. Hu and G. D. Stucky, *Nano Energy*, 2019, **56**, 828–839.

61 X. Li, X. Sun, Z. Gao, X. Hu, R. Ling, S. Cai, C. Zheng and W. Hu, *ChemSusChem*, 2018, **11**, 1549–1557.

62 Y. Chen, X. Hu, B. Evanko, X. Sun, X. Li, T. Hou, S. Cai, C. Zheng, W. Hu and G. D. Stucky, *Nano Energy*, 2018, **46**, 117–127.

63 M. Cuisinier, P.-E. Cabelguen, S. Evers, G. He, M. Kolbeck, A. Garsuch, T. Bolin, M. Balasubramanian and L. F. Nazar, *J. Phys. Chem. Lett.*, 2013, **4**, 3227–3232.

64 T. Z. Hou, W. T. Xu, X. Chen, H. J. Peng, J. Q. Huang and Q. Zhang, *Angew. Chemie - Int. Ed.*, 2017, **56**, 8178–8182.

65 M. U. M. Patel, I. Arčon, G. Aquilanti, L. Stievano, G. Mali and R. Dominko, *ChemPhysChem*, 2014, **15**, 894–904.

66 X. Liang, C. Y. Kwok, F. Lodi-Marzano, Q. Pang, M. Cuisinier, H. Huang, C. J. Hart, D. Houtarde, K. Kaup, H. Sommer, T. Brezesinski, J. Janek and L. F. Nazar, *Adv. Energy Mater.*, 2016, **6**, 1501636.

67 Q. Pang, D. Kundu, M. Cuisinier and L. F. Nazar, *Nat. Commun.*, 5, 4759

68 X. Liang, C. Hart, Q. Pang, A. Garsuch, T. Weiss and L. F. Nazar, *Nat. Commun.*, 2015, **6**, 5682.

Table of Contents Entry